INTERNATIONAL JOURNAL FOR NUMERICAL METHODS IN FLUIDS, VOL. 4, 619–640 (1984)

A MODIFIED FINITE ELEMENT METHOD FOR SOLVING THE TIME-DEPENDENT, INCOMPRESSIBLE NAVIER–STOKES EQUATIONS. PART 2: APPLICATIONS*

PHILIP M. GRESHO, STEVENS T. CHAN, ROBERT L. LEE AND CRAIG D. UPSON
Atmospheric and Geophysical Sciences Division, Lawrence Livermore National Laboratory, Livermore, CA 94550, U.S.A.

SUMMARY

Three examples will be presented to demonstrate the performance of the scheme described in Part 1 of this paper.[1] Two are isothermal ($T = 0$) and two-dimensional, and one of these is steady and the other time-dependent. The third example involves buoyancy effects, is time-dependent and three-dimensional, and is presented in less detail. The paper concludes with a short discussion and some conclusions from both Parts 1 and 2.

CONTENTS

1. NUMERICAL RESULTS

1.1. Lid-driven cavity

We selected this 'classic' example because there appears to be a new 'standard', at high *Re*, against which many results will probably be compared for some time to come. In the work by Ghia *et al.*[2], a series of detailed fine-mesh results has been presented for $Re = 100$, 400, 1000, 3200, 5000, 7500 and 10,000. Herein we will compare against their high *Re* (≥ 1000) results, obtained with a very fine, but uniform mesh (129×129 nodal points for $Re \leq 3200$ and 257×257 points for $Re \geq 5000$). Since they used a stream function/vorticity approach, our primitive variable results are complementary to theirs (they present stream function and vorticity contours and we will present pressure contours and vector fields—as well as streamlines).

---

* This invited paper is an extended, and refereed version of one presented at the Fourth International Symposium on Finite Elements in Flow Problems held in Tokyo, Japan, 26–29 July, 1982.

0271–2091/84/070619–22$02.20

Received 16 May 1983
Revised 1 December 1983

Another reason for choosing this example is that we believed that a good mesh design would yield similar accuracy using our modified FEM and significantly fewer nodal points. We *a priori* selected a mesh of 50×50 elements (2601 node points vs 65,536) and designed it to capture the details in the corners and in the boundary layers (for $Re \leq 7500$; we 'pushed it' to $Re = 10{,}000$). We believed that we could tolerate large elements in the cavity centre since the flow is presumably simple to model away from the walls and corners. As it turned out, our mesh is probably very good, but probably not optimal (are they ever?) nor quite fine enough. The smallest element size has $h = 0{\cdot}005$ (the 4 corners); the mesh is graded symmetrically and the four largest elements at the centre of the cavity have $h = 0{\cdot}060$ and the largest aspect ratio is 12—at the centre of and near each wall. The average element size is (of course) 0·02 whereas in Reference 2 it is uniform at ~0·0039. Since the flow is nearly one-dimensional near the walls, we used (35)* to estimate the stability limit; conservatively, using $u = 1$ near the corner at the lid gives $\Delta t \leq \sim 0.004$–0.005 for all Re of interest; all simulations were done using $\Delta t = 0{\cdot}005$. (Without BTD, the Δt limits would have been ~0·002 at $Re = 1000$ and ~0·0002 at $Re = 10{,}000$.) The grid Reynolds numbers (at the lid) ranged from a low of ~2·5 for $Re = 1000$ (near the corners) to ~300 for $Re = 10{,}000$ (near the centre). The boundary conditions are: $v = 0$ everywhere and $u = 0$ everywhere except on the top lid, where $u = 1$ 'almost everywhere' ($u = 0$ at the corners and $u = \frac{1}{2}$ at the first node in from the corners, to respect the 'spurious CB constraint' described by Sani *et al.*[3].

We present detailed results only for $Re = 5000$ and 10,000 (for other values of Re, see Reference 2). Figures 1 and 2 show the stream function contours for the entire (unit) cavity and corner enlargements ($0{\cdot}4 \times 0{\cdot}4$) with the velocity field superimposed. Overall, these figures compare rather well with those of Ghia *et al.* except for one region: the lower right eddies at $Re = 10{,}000$. Our results seem to predict the wrong size and shape of the small eddy (the one with clockwise circulation), a point we shall return to later.

The isobars for these two cases are shown in Figures 3 and 4, where the reference pressure was taken to be zero at the lower left corner and the spurious chequerboard pressure mode was filtered via 'scheme 3' (element area weighting) described by Sani *et al.*[3] It is noteworthy for these high Reynolds numbers that the isobars seem to nearly satisfy $\partial P/\partial n = 0$ at the walls, even in the recirculation zones. This is consistent with the Neumann boundary conditions associated with (5), derived from (1a), for $Re \gg 1$. The highest pressures in the upper right corner are not plotted since they would obscure the vector field and are not particularly interesting (i.e. concentric circles, more or less).

The final contours, presented in Figure 5, are those for total pressure, $P_T = P + \rho(u^2 + v^2)/2$, where P is the (static) pressure computed from the NS equations. The interesting point to be made here is that, in the region of the main vortex, these contours coincide with those of the stream function, consistent with inviscid flow (Euler's equations), for which P_T is constant along a streamline (à la Bernoulli). The trend towards this behaviour was already detected by Burggraf[4] at $Re = 400$, and in our results, at $Re \gtrsim 5000$, it even tends to occur in the first lower right eddy (for which the eddy Reynolds number is ~400 at $Re = 10{,}000$). Note that the regions just below the lid and slightly away from the right wall are (purposely) devoid of plotted contours, since the total pressure (and ∇P_T) is quite large there; the velocity in this region is also interesting, as we see below.

Figure 6 shows velocity profiles through the centre of the cavity at $Re = 10{,}000$, which agree well with those of Ghia *et al.* and display similar 'kinks' in the same regions discussed above; one in $u(y)$ near $y = 0{\cdot}95$ or so and one in $v(x)$ *at* $x \simeq 0{\cdot}95$. These are also regions of

* Equation numbers refer to the equations of Part 1 of this paper.[1]

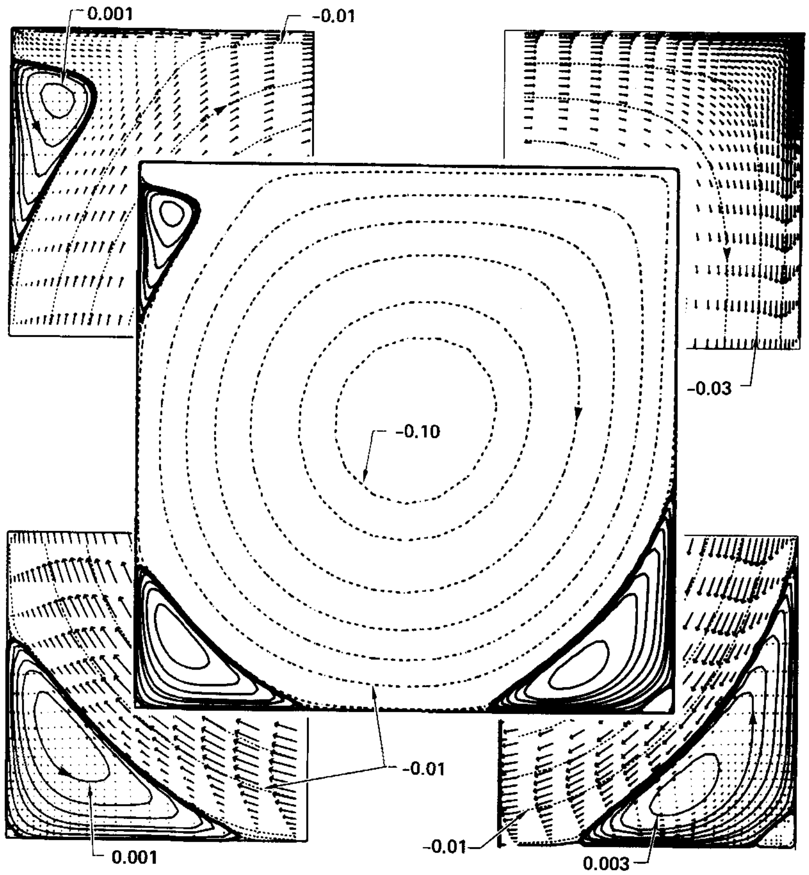

Figure 1. Flow field at $Re = 5000$; solid curves are $\psi > 0$, dashed are $\psi < 0$. Contours (full cavity) are: $-0{\cdot}10$, $-0{\cdot}09$, $-0{\cdot}07$, $-0{\cdot}05$, $-0{\cdot}03$, $-0{\cdot}01$, $-0{\cdot}0001$

large vorticity gradients[2] and the interesting behaviour in this region appears to be related to the rapid transition from boundary layer flow to inviscid core flow. We must add, however, that this behaviour seems to occur only in 2D since Koseff *et al.*[5] do not see it in 3D laboratory experiments. Indeed, their measured velocity profiles disagree substantially with those in Figure 6; as these authors point out, 3D cavities can differ greatly from their 2D counterparts.

To obtain some more quantitative comparisons with Ghia *et al.*, Tables I and II show the local extrema in stream function and velocity, respectively, from both simulations, and we shall regard their results as 'truth'. Our mesh is apparently not fine enough to correctly capture the total flow (Table I) in the various eddies, e.g. we are consistently low in the primary vortex (2–16 per cent), (nearly) consistently high in the two main lower corner eddies (10–27 per cent for the bottom left and 1–62 per cent for the bottom right), and consistently low (8–20 per cent) in the top left eddy. The velocity extrema look better, however; the error in u is ≤ 2 per cent and that in v is < 4 per cent, although the locations of the extrema are not as good. (Also noteworthy in this Table is that not even the fine grid results of Ghia *et al.* exhibit monotonic behaviour of these extrema.)

Turning briefly to the cost of these simulations, we first mention that we have only one 'clean' result: the run at $Re = 1000$ started from rest and achieved 'steady state' (which we

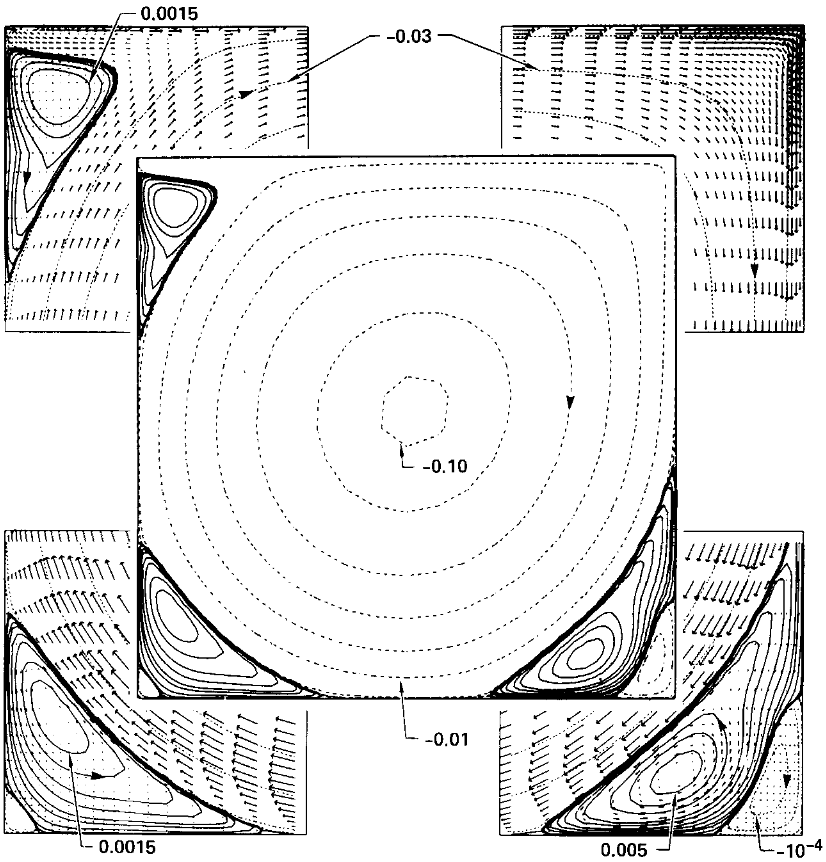

Figure 2. Same as Figure 1 except $Re = 10{,}000$

avoid defining very carefully) by $t = 30$; this true time-dependent simulation required ~70 s of CPU to march 6000 minor time steps and 240 major time steps (average subcycle ratio of 25). By comparison, Ghia *et al.* required 90 s (on a 129×129 mesh) to achieve the 'same' steady state (via an efficient multi-grid method) using an AMDAHL 470 V/6 computer, reported to five times slower than a CDC-7600 (K. Ghia, personal communication), which translates (roughly) to ~20 times slower than our CRAY-1, i.e. it would require only ~4·5 s on the CRAY-1. Thus, we appear to be paying a factor of ~15 in CPU cost to obtain a fully time-dependent solution, which may or may not be worth while. (Recall that our method has been designed with transient simulations in mind; steady-state results, when they exist, are perhaps better regarded as a 'bonus'.) For $Re = 10^4$, Ghia *et al.* report (for the 257×257 grid) upwards of 20 min CPU, i.e. about 1 min on the CRAY-1. Although we do not have very good timing data for this case (we did not start from rest and perform the full transient simulation), we believe that a similar ratio (10 or so) would again occur if we did start from rest. For this extra cost however, we obtain in addition to the full transient, an important additional piece of data, not obtainable by steady-state solution techniques: the steady-state solution *exists*, i.e. it is stable. Finally we remark that the timing reported by Ghia *et al.* did not include the cost of finding the optimum set of multi-grid 'tuning parameters'; presumably

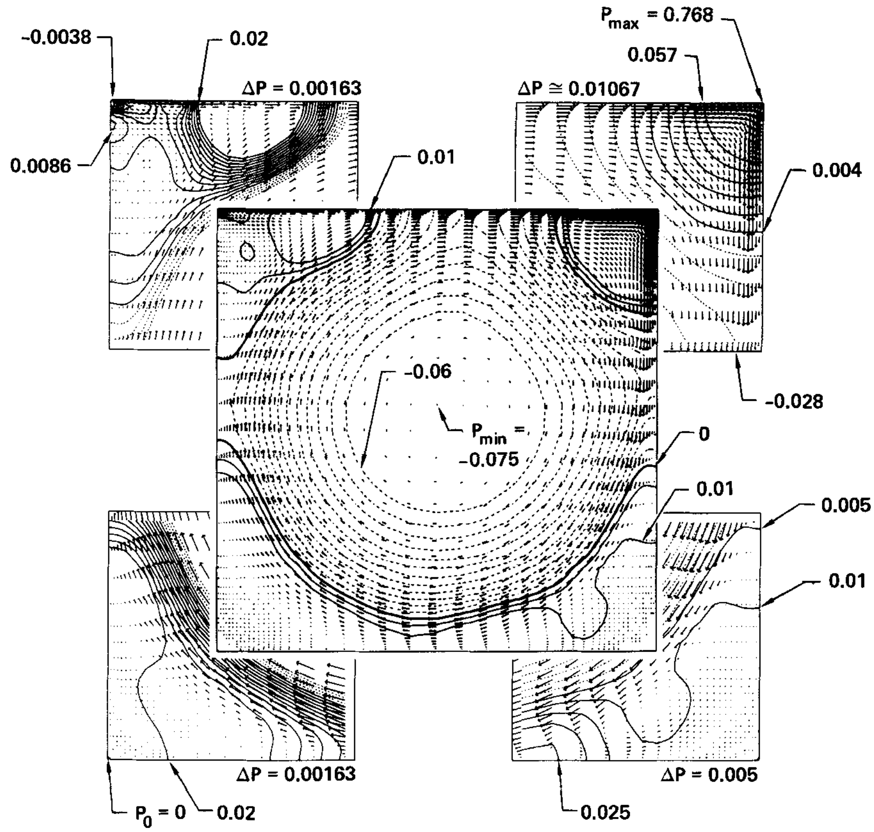

Figure 3. Isobars and velocity vectors for $Re = 5000$; solid curves are $P > 0$, dashed are $P < 0$. Contours (full cavity) are: $-0{\cdot}06\ (0{\cdot}005)\ 0{\cdot}01$

this cost is either negligible or the same parameters can be used for other simulations (or both).

A few remarks regarding Stokes flow, corner singularities and Moffatt's eddies[6,4] may be also in order:

(i) Even though the corner singularities are analytically describable by assuming Stokes flow near the corners,[7,8] the realization of this zero-inertia limit does not appear to be possible for large Re without extreme mesh refinement in these corners. For example, the pressure solution in the top right corner is[7]

$$P(r, \theta) = \frac{4}{Re(\pi^2 - 4)} (\pi \sin \theta + 2 \cos \theta)/r$$

where r is the (dimensionless) distance from the corner and θ is the angle from the top lid. In order for this $1/r$ description to be accurate, we need to be sufficiently close to the corner that $rRe \ll 1$, which translates to, e.g. $r \ll 10^{-4}$ for $Re = 10^4$ (vis-à-vis $\Delta x = 0{\cdot}0039$ on the best grid of Ghia *et al.*). We should also remark that Winters and Cliffe and, more recently, Hutton[9] present a rather strong argument for performing detailed grid refinement in the top corners for this problem. Although we probably should have heeded this good advice, we took the cheaper route so that we could use

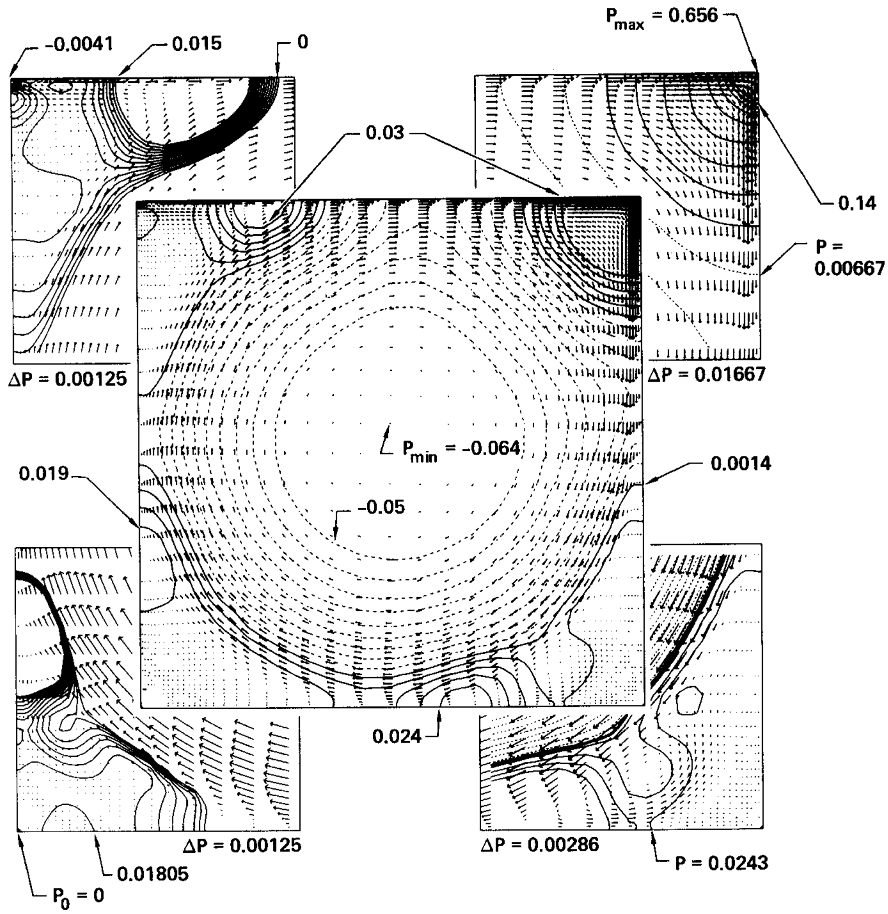

Figure 4. Same as Figure 3 except $Re = 10{,}000$ and contours (full cavity) are: −0·05 (0·00571) 0·03

the more efficient version of our code which is restricted to logically-regular meshes. (Non-logical meshes cause a loss of efficiency since they require extensive use of non-vectorizable instructions.) Perhaps we will later investigate the effect of corner mesh refinement. We hope that the numerical results (ours, and those of Ghia *et al.*) are still meaningful away from these corners and that the highly local singularity does not affect the overall solution too much (but cf. Reference 9).

(ii) The multiple eddies in the lower corners appear to be related to the sequence of Stokes flow eddies (initially) studied by Moffat,[6] although there appears to be a slight paradox: Re must be increased to generate multiple eddies, yet their presence is predicted by assuming $Re \rightarrow 0$. (However, Burggraf[4] found good agreement with Moffatt's theory at $Re = 400$ for the (single) eddy in the lower right corner).

In summary and conclusion, we offer:

(i) For the 'overworked' and somewhat controversial 2D lid-driven cavity problem, we see the interesting result (already noted, in part, by Burggraf[4]) that nearly all ranges of behaviour of the NS equations can be displayed: Stokes flow (very) near the corners, fully viscous flow near the walls and in most of the eddies, and nearly inviscid

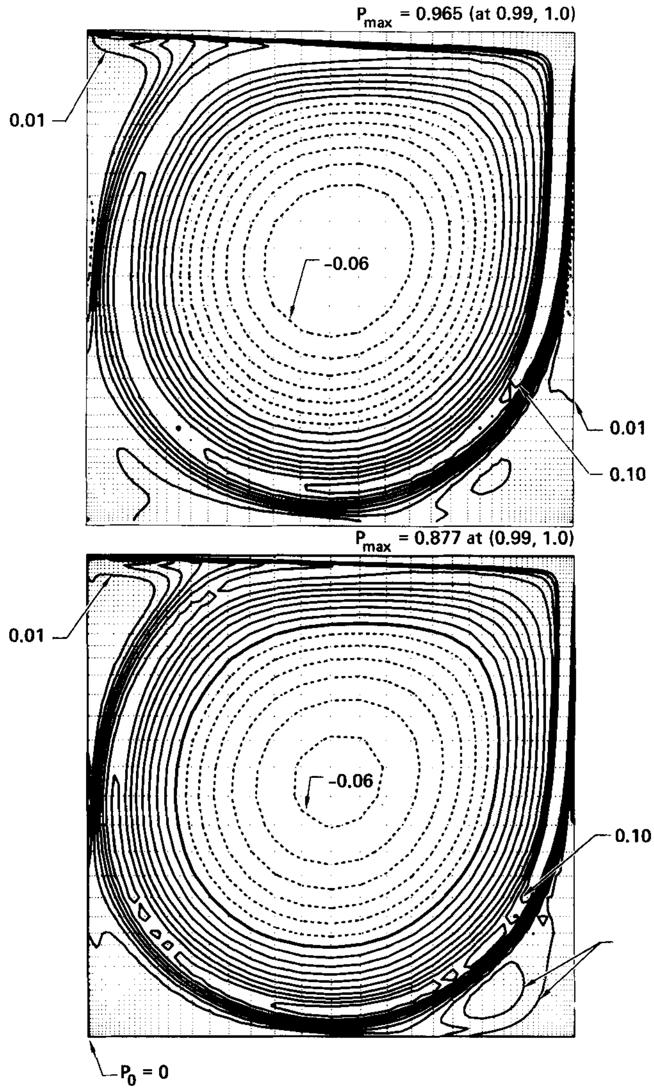

Figure 5. Total pressure fields; solid curves are $P_T>0$, dashed are $P_T<0$. Top: $Re=5000$; bottom: $Re=10,000$. Contour interval is 0·01

flow (with constant vorticity) in the primary eddy. Perhaps this heavily-studied model problem is indeed worth while, in spite of the corner singularities.

(ii) For the most part, our results (on a relatively coarse mesh) compare well with the fine mesh results of Ghia *et al.*—the notable exception being the shape and strength of the bottom right eddies at the highest Re (10^4).

(iii) Our results demonstrate (nearly) that stable steady-state laminar solutions exist, at least up to $Re=10^4$. (This result does not carry over to 3D, however, since Koseff and Street[10] report a breakdown of steady laminar flow at $Re \simeq 6000$–8000 in a 3D cavity with a 3:1 aspect ratio.)

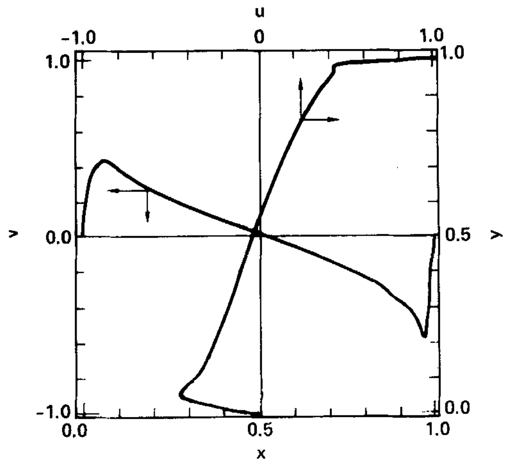

Figure 6. Velocity profiles through the centre of the cavity; $Re = 10{,}000$

Table I. Stream function extrema

Re	Primary vortex	Top left	Bottom left 1	Bottom left 2	Bottom right 1	Bottom right 2	
	$-0{\cdot}114$	—	$2{\cdot}0\times10^{-4}$	$-1{\cdot}14\times10^{-9}$	$1{\cdot}76\times10^{-3}$	$-1{\cdot}8\times10^{-8}$	Present work
1000	$-0{\cdot}118$	—	$2{\cdot}31\times10^{-4}$	—	$1{\cdot}75\times10^{-3}$	$-9{\cdot}32\times10^{-8}$	Ghia *et al.*
	$-0{\cdot}118$	$5{\cdot}86\times10^{-4}$	$1{\cdot}20\times10^{-3}$	$-1{\cdot}00\times10^{-8}$	$3{\cdot}29\times10^{-3}$	$-2{\cdot}05\times10^{-7}$	Present work
3200	$-0{\cdot}120$	$7{\cdot}28\times10^{-4}$	$9{\cdot}78\times10^{-4}$	$-6{\cdot}33\times10^{-8}$	$3{\cdot}14\times10^{-3}$	$-2{\cdot}22\times10^{-7}$	Ghia *et al.*
	$-0{\cdot}109$	$1{\cdot}23\times10^{-3}$	$1{\cdot}49\times10^{-3}$	$-2{\cdot}85\times10^{-8}$	$3{\cdot}87\times10^{-3}$	$-5{\cdot}22\times10^{-8}$	Present work
5000	$-0{\cdot}119$	$1{\cdot}46\times10^{-3}$	$1{\cdot}36\times10^{-3}$	$-7{\cdot}09\times10^{-8}$	$3{\cdot}08\times10^{-3}$	$-1{\cdot}43\times10^{-6}$	Ghia *et al.*
	$-0{\cdot}108$	$1{\cdot}84\times10^{-3}$	$1{\cdot}75\times10^{-3}$	$-2{\cdot}74\times10^{-7}$	$4{\cdot}86\times10^{-3}$	$-7{\cdot}46\times10^{-5}$	Present work
7500	$-0{\cdot}120$	$2{\cdot}05\times10^{-3}$	$1{\cdot}47\times10^{-3}$	$-1{\cdot}83\times10^{-7}$	$3{\cdot}28\times10^{-3}$	$-3{\cdot}28\times10^{-5}$	Ghia *et al.*
	$-0{\cdot}101$	$2{\cdot}23\times10^{-3}$	$1{\cdot}93\times10^{-3}$	$-3{\cdot}08\times10^{-8}$	$5{\cdot}54\times10^{-3}$	$-2{\cdot}02\times10^{-4}$	Present work
10,000	$-0{\cdot}120$	$2{\cdot}42\times10^{-3}$	$1{\cdot}52\times10^{-3}$	$-7{\cdot}76\times10^{-7}$	$3{\cdot}42\times10^{-3}$	$-1{\cdot}31\times10^{-4}$	Ghia *et al.*

1.2. Vortex shedding behind a cylinder

We next present some results for another classic problem: flow past a circular cylinder. We will present some detailed results in the vortex shedding regime at $Re = u_0D/\nu = 50$ and 200, and less detailed results at $Re = 100$ and 400. Finally, we will show results in a case where a steady-state solution is attained ($Re = 25$). The computational domain, shown in Figure 7, is about 21 units long (length is measured in cylinder diameters) and about 9 units high. The general mesh design follows that of Brooks and Hughes,[11] which improved our

Table II. Extrema in velocity

	Present work						Ghia *et al.*					
Re	U_{min} $(x=0\cdot5)$		V_{min} $(y=0\cdot5)$		V_{max} $(y=0\cdot5)$		U_{min} $(x=0\cdot5)$		V_{min} $(y=0\cdot5)$		V_{max} $(y=0\cdot5)$	
	U_{min}	y	V_{min}	x	V_{max}	x	U_{min}	y	V_{min}	x	V_{max}	x
1000	−0·375	0·160	−0·516	0·906	0·362	0·160	−0·383	0·172	−0·516	0·906	0·371	0·156
3200	−0·420	0·084	−0·560	0·945	0·415	0·094	−0·419	0·102	−0·541	0·945	0·428	0·094
5000	−0·426	0·074	−0·563	0·906	0·419	0·074	−0·436	0·070	−0·554	0·953	0·436	0·078
7500	−0·430	0·055	−0·567	0·963	0·424	0·064	−0·436	0·063	−0·552	0·960	0·440	0·070
10,000	−0·431	0·055	−0·559	0·963	0·423	0·064	−0·427	0·055	−0·543	0·969	0·440	0·063

earlier mesh[12] except that our current mesh is somewhat finer since it was designed for $Re \leq \sim 400$ (based on estimated boundary layer thickness, vortex spacing, etc.). We used 1760 elements (1852 nodes) with a graded mesh (see Figure 8 for mesh details near the cylinder). Denoting r as the radial co-ordinate and θ as the angular co-ordinate, the minimum Δr is $\sim 0{\cdot}027$, and Δr gradually grows to $\sim 0{\cdot}3$ (attained at ~ 4 diameters behind the cylinder on the centreline), which is then constant to the outlet. In the circumferential direction, $r\Delta\theta$ is constant at 0·078 over the front half and 0·044 over the rear half (on the cylinder surface). The boundary conditions were chosen to approximate tow tank conditions: $u = u_0 = 1$, $v = 0$ at the inlet and along the top and bottom walls; natural boundary conditions were used at the exit (namely, $-P + Re^{-1}\,\partial u/\partial x = 0$ and $\partial v/\partial x = 0$). The minor time step used was usually 0·05 which corresponds to ~ 60 steps per half shedding cycle (recall that the horizontal velocity in the wake oscillates at twice the shedding frequency). The Δt algorithm would have used a subcycle ratio of only about 3 (giving 20 major steps per one-half cycle, a reasonable number). Thus, we decided not to use the subcycle option at all since the gain in cost-effectiveness is very small.

We present first a series of streamline snapshots for $Re = 50$, 100, 200 and 400 at (approximately) the same point in time during vortex shedding in Figure 9; the 'same time'

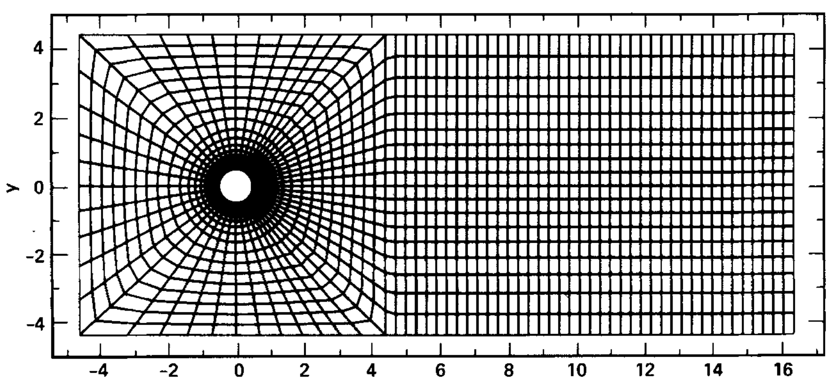

Figure 7. Finite element mesh for flow past a cylinder

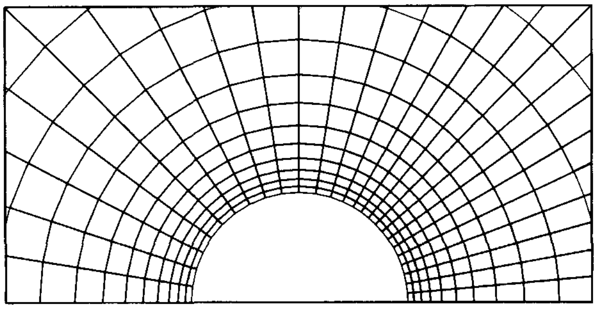

Figure 8. Mesh details near cylinder

corresponds (approximately) to the first appearance of the attached eddy on the top re portion of the cylinder. The wavelengths for these cases are 6·5, 5·2, 4·4 and 4·4 respectively, where we also note that, unlike the results presented earlier on a too-coarse mesh (at $Re = 100$; see Reference 13) wherein the vortices tended to cross over the wake centreline and even disappear, these results appear to be much more reasonable. (Snapshots of relative streamlines, not presented, show that the vortices remain on the same side of the centreline as that of their genesis.) We now attribute the earlier failure to the combined effects of: (i) the pressure gradient error associated with a coarse mesh of distorted elements and (ii) large phase error on the same mesh—both of which are much-reduced in the present set of calculations.

Denoting by τ the period for one shedding cycle (during which two vortices are shed—one from the top and one from the bottom), Figures 10 and 12 depict a sequence of streamline snapshots covering half of a cycle ($\Delta t = \tau/16$) for $Re = 50$ and 200, respectively (also shown

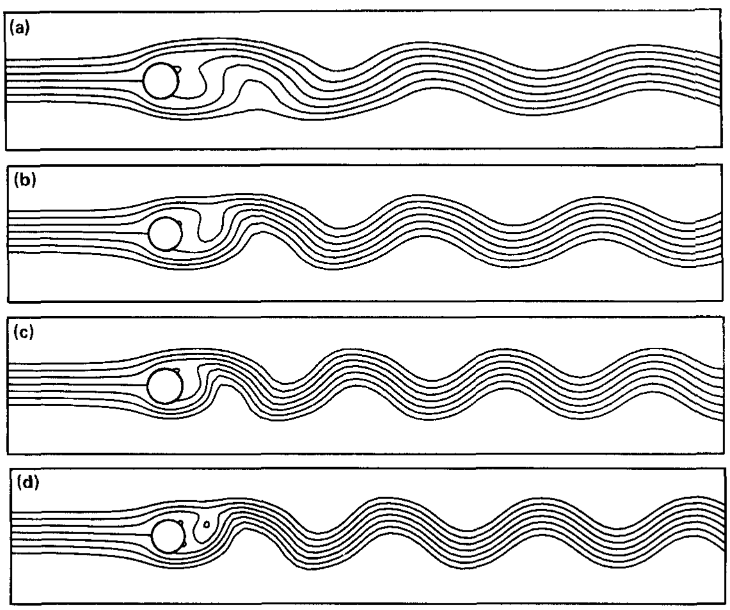

Figure 9. Streamlines during quasi-steady vortex shedding; contour values are: 0, ±0·2, ±0·4, ±0·6. (a) $Re = 50$; (b) $Re = 100$; (c) $Re = 200$; (d) $Re = 400$

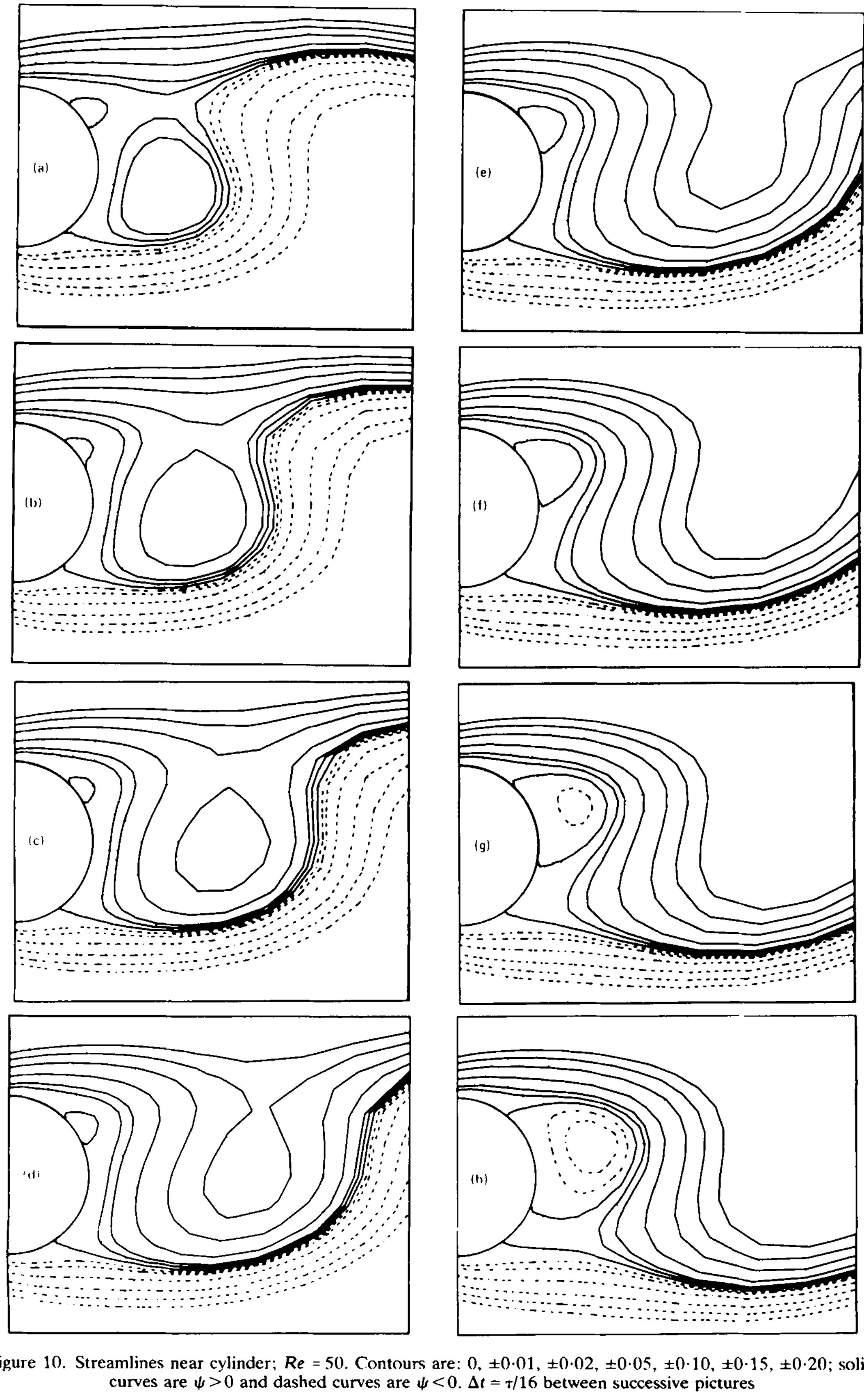

Figure 10. Streamlines near cylinder; $Re = 50$. Contours are: 0, $\pm 0{\cdot}01$, $\pm 0{\cdot}02$, $\pm 0{\cdot}05$, $\pm 0{\cdot}10$, $\pm 0{\cdot}15$, $\pm 0{\cdot}20$; solid curves are $\psi > 0$ and dashed curves are $\psi < 0$. $\Delta t = \tau/16$ between successive pictures

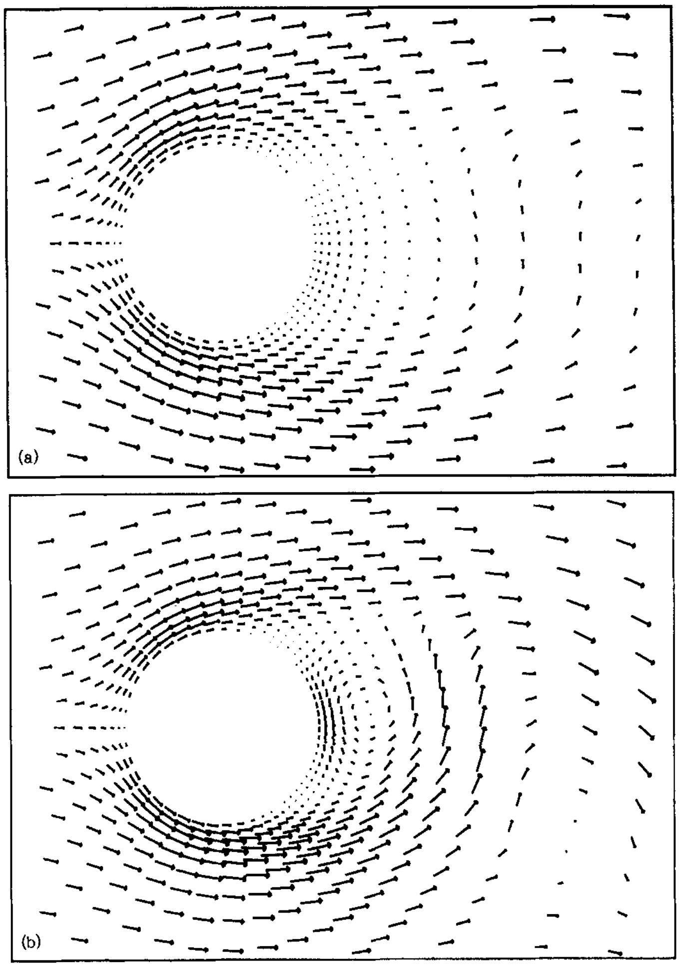

Figure 11. Velocity field near cylinder at $t = 0$ at $Re = 50$ (a) and $Re = 200$(b)

in Figure 11 are the velocity vectors corresponding to the first of the streamline plots); again $t = 0$ is chosen to be the first clear appearance of the top vortex. The differences between the two sets of results are interesting: (i) whereas the new vortex exhibits monotonic growth, and finally, detachment at $Re = 50$, the 'same' vortex at $Re = 200$ seems to grow slightly, then shrink in size (perhaps even disappearing then reforming), and finally grows monotonically in size and strength before detaching, (ii) the time history plots near the cylinder for this latter case (indeed for all $Re \geq 200$) are consistent with these pictures in that multiple frequencies are present (two for $Re = 200$ and 400; many for $Re = 1000$), (iii) the 'formation region' is much 'tighter' and closer to the cylinder for the higher Re and the eddy is more vertical than horizontal, and (iv) the magnitude of the velocity in this near-wake region is significantly higher for $Re = 200$ than for $Re = 50$.

Turning now to a summary of all vortex shedding results, we refer to Tables III and IV for some quantitative data. The principal observations we make are the following:

(1) The Strouhal number ($St = u_0 f/D$, where $f = 1/\tau$ is the shedding frequency) appears to be somewhat high relative to the available experimental data.

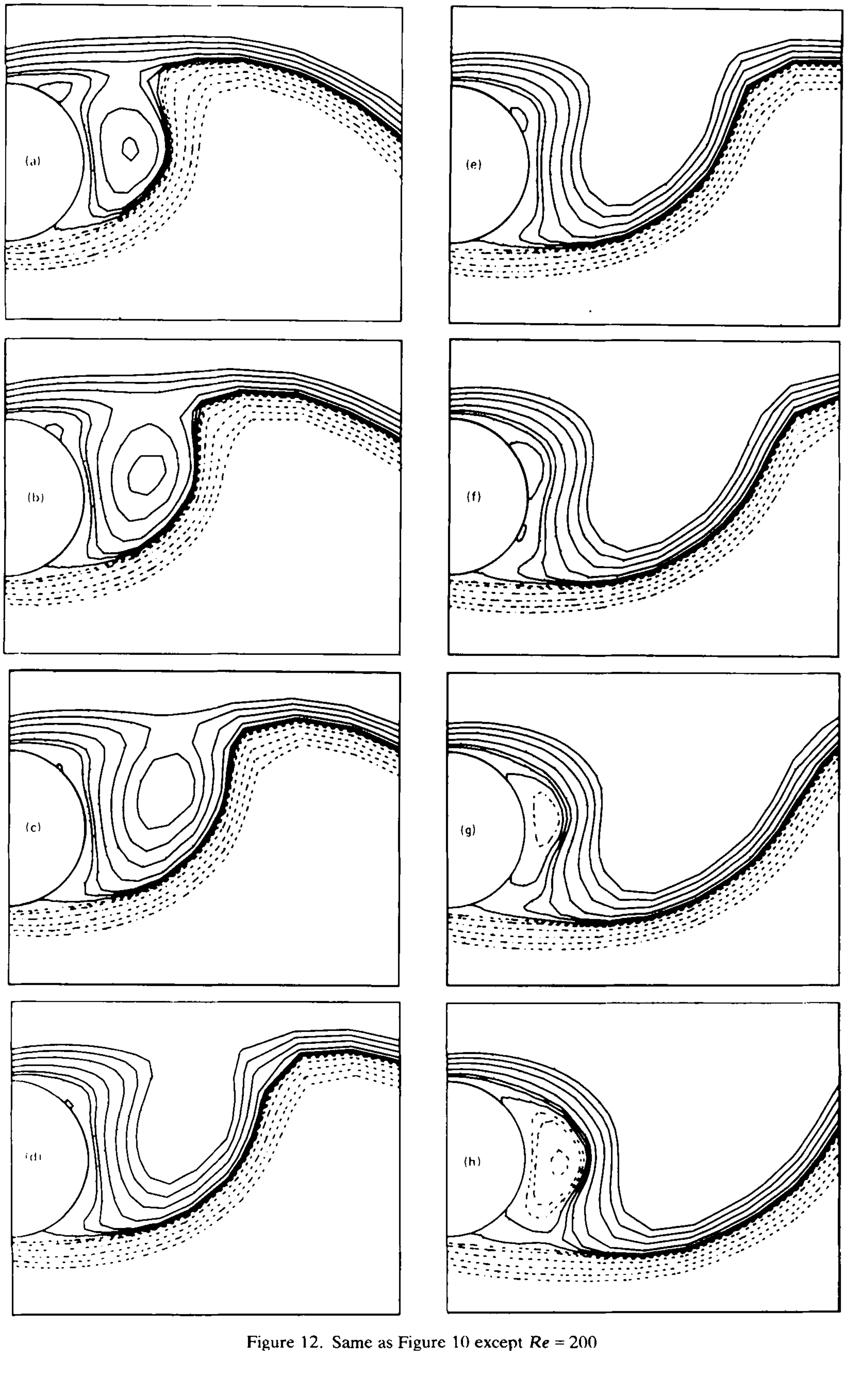

Figure 12. Same as Figure 10 except $Re = 200$

Table III. Summary of vortex shedding results

Re	Period (τ)	Strouhal No. ($1/\tau$)	Wave-length (λ)	Vortex speed (λ/τ)	Drag coefficient, C_D: Average	Drag coefficient, C_D: Peak-to-Peak	Lift coefficient (Peak-to-peak)	Range of u_8*	Range of v_8*	Range of $\lvert\mathbf{u}\rvert_{max}$†
25	—	—	—	—	2·26	0	0	0·59	0	1·31
50	7·0	0·14	6·5	0·93	1·81	0·01	0·69	0·76–0·87	±0·44	1·36–1·39
100	5·6	0·18	5·2	0·93	1·76	0·07	1·48	0·86–0·94	±0·62	1·44–1·51
200	4·8	0·21	4·4	0·92	1·76	0·18	2·10	0·93–0·98	±0·77	1·53–1·64
400	4·6	0·22	4·4	0·96	1·78	0·38	2·82	1·0048–1·0050	±0·85	1·64–1·77
50‡	7·1	0·14	6·4	0·90	1·71	0·0005	0·14	0·56–0·69	±0·27	~1·33

* $\mathbf{u}_8$ is the velocity on the centreline ~8 diameters downstream of the cylinder.
† $\lvert\mathbf{u}\rvert_{max}$ is the maximum speed in the domain; it typically occurs ~1 diameter above the cylinder.
‡ 9-node element (4-node bilinear pressure) via GFEM, using the (coarser) mesh discribed by Gresho *et al.*[1,13]

(2) The drag coefficients are also higher than the experimental values (experimental values for the lift coefficient are difficult to find), e.g. Jordan and Fromm[14] show values of c_D of about 2·0, 1·5, 1·3, 1·2 and 1·2 for the 5 values of Re in Table III.
(3) The pressure contribution was 70–80 per cent of the total lift and drag, in reasonable agreement with the results of Swanson and Spaulding.[15]
(4) For the most part, the solution at $Re = 50$ agrees well with that from a higher order element using GFEM (3×3 quadrature, consistent mass, same BCs), although the lift coefficient and the overall 'intensity' of the flow are noticeably larger for the 4-node element.

The calculation at $Re = 50$ with the 9-node element was performed in order to assess, in part, the ostensibly inaccurate results (again) from the 4-node element; partly for c_D and Strouhal number, but partly for another reason: experimentalists report[16–20] the existence of two permanently *attached* (and presumably oscillating and unsymmetric) eddies at this value of Re (and, indeed, at any $Re < Re_c$ where Re_c is variously reported as ~90–110). The 9-node results also clearly 'showed' that vortex shedding occurs (no permanently attached eddies) at this low Re, thus bolstering our confidence in the 4-node results while at the same time leaving us somehwat puzzled. Why does a pair of eddies remain attached in the physical laboratory and not in the computer laboratory? We regret that we do not yet have a good answer—only guesses, and these are more or less the obvious ones (mesh too coarse, domain too small, poor choice of BCs, etc.). The only investigators we have found who seem to agree

Table IV. Comparison of calculated and measured Strouhal numbers

Re	Our calculation	Berger & Wille[18]	Gerrard[20]: Figure 1	Gerrard[20]: Figure 2	Gerrard[20]: From recommended equation
50	0·14	0·12–0·13	0·14	0·13	0·12
100	0·18	0·16–0·17	0·17	0·15	0·16
200	0·21	0·18–0·19	0·18–0·20	0·18	0·18
400	0·22	0·20–0·21	0·20–0·21	0·20	0·20

with us are Perry *et al.*[21] who, in spite of the laboratory results referred to above, propose (their Figure 2) that a mechanism much like that shown in Figures 10 and 12, 'is valid irrespective of the Reynolds number'. Perhaps in the future we (or, we hope, someone else) will add a streakline capability and repeat some of these simulations (using a finer mesh and a larger computational domain), to see if the Perry *et al.* model is 'correct' (see their Figure 9).

To further examine the accuracy (or otherwise) of our model, we doubled the viscosity to cause a step reduction in Re from 50 to 25 and continued the integration. The oscillatory behaviour decayed slowly and monotonically, reaching a steady state by 50–60 time units ($t \sim D/u_0$). The good news was that the steady state exhibited a pair of symmetric attached eddies, the detailed structure of which agreed very well with the experimental results of Coutanceau and Bouard;[22] see Table V. The principal conclusion we draw from this comparison is that our results are sufficiently accurate, at least for the steady case. If the high Re cases, with vortex shedding, are erroneous, it may be that it is only the dynamic case that is particularly sensitive to errors in ∇P and that these errors may in fact cancel in the steady state owing to the symmetry about the centreline. (Recall also that in Reference 13 we reported that the 4-node and 9-node results from a steady-state code agreed quite well at $Re = 100$ on a much coarser mesh; the symmetric eddy pair was then ~4·5 diameters long).

Table V. Comparison of steady state results for $Re = 25$

	Experiments of Coutanceau and Bouard[22]		
	$\lambda = 0{\cdot}12$*	$\lambda = 0{\cdot}0$†	Present study
Length of closed wake measured from the rear of cylinder	0·90	1·22	1·15
Maximum width of the wake	0·73	0·85	0·81
x-co-ordinate of the maximum width of the wake‡	0·63	0·75	0·67
Separation angle from the x-axis	45°	48°	45°
x-co-ordinate of vortex centre	0·82	0·94	0·88
Vertical distance between vortex centres	0·44	0·51	0·47
Maximum velocity on the x-axis in the closed wake (toward cylinder)	0·047	0·057	0·057
x-co-ordinate of the maximum velocity	0·87	1·00	0·99

* λ is the ratio between the cylinder and tank diameters.
† Results corresponding to $\lambda = 0$ were obtained by Coutanceau and Bouard via extrapolation.
‡ The origin of coordinate system is at the centre of the cylinder and length is in units of cylinder diameter.

Additional remarks

(i) When we changed the inlet BC from $u = 1$ to one of specified force, $f_n(y)$ ($Re \simeq 100$), the inlet velocity profile was altered and the drag coefficient reduced from 1·76 to ~1·37, in much better agreement with experiments. This suggests that our inlet is too close to the cylinder to use tow tank BCs for vortex shedding (recall that the $Re = 25$ results are good), and this may explain a large part of the discrepancy between our results and those of others.

(ii) The boundary layer on the upstream portion of the cylinder seems to be adequately resolved (Figure 11); this is also true at $Re = 400$.

(iii) If, in fact, all of the following quantities: shedding frequency, lift, drag, and velocity in the wake are too large, there is probably a common cause.

Turning briefly to the higher *Re* results, we first recall that some time histories displayed multiple frequencies for $Re \gtrsim 200$. Indeed, an attempt to simulate $Re = 1000$ seemed to be trying to show multiple and ephemeral small-scale vortices in the immediate vicinity of the cylinder—and there was no tendency to form a clear vortex street nor even to attain a quasi-steady oscillatory solution. These effects may be related to the basic instability of laminar flow at higher *Re*. For example, Bloor[23] observed what appeared to be a two-dimensional transition to turbulence via Tollmein–Schlichting waves for $Re \gtrsim 400$, about which she states, 'Above $Re = 400$ transition occurs before the separated layer rolls up, the vortices once formed being turbulent', and 'Turbulence, when it develops in the separated layers, is preceded by two-dimensional Tollmein–Schlichting waves which eventually degenerate to turbulence by the action of small-scale three-dimensionalities'. Perhaps our 2D difficulties at $Re = 1000$ are related to these experimental observations.

While on the subject of laboratory results, let us conclude by noting that the experimentalists also do not yet have all the answers and often disagree with each other; examples:

(1) Tritton[16,24] and others[18,25,26] seem to believe that there is a discontinuity in the *St–Re* curve at $Re \simeq 100$ and an associated change in the physics. Gaster[27,28] disagrees and claims that the behaviour is smooth (the 'Tritton–Gaster controversy'[18]).

(2) Related to this, Gerrard[20] notes that even Tritton[16] and Berger[25] disagree on the direction of the discontinuity as *Re* is increased; Tritton predicts a sudden decrease in *St* and Berger a sudden increase.

(3) The origin of the instability leading to the periodic oscillations in the wake at $Re \gtrsim {\sim}40$ is (to our knowledge) not yet agreed upon; e.g. Tritton[16,17] blames it on 'an instability of the wake; the only role of the cylinder is to produce the velocity profile'. Gerrard[20] argues, however, that the separation bubble itself becomes unstable and forms waves or 'gathers' which ultimately become unstable.

(4) If, during vortex shedding at $Re \sim 100$, dye is injected upstream of the cylinder and slightly away from the centreline, Zdravkovich[19] claims (and his photos seem to support) that the dye may actually end up on the other side of the centreline in the downstream wake and vortices. Gerrard,[20] however, disagrees and claims that the dye would end up in the vortices on the same side of the wake. It should be noted, however, that Gerrard performed a different experiment—he injected (or generated) dye in the near-wake.

Thus, although the computer laboratory is plagued with issues numerical in nature, the physical laboratory seems also to be far from perfect. To some extent, it seems that the more we study this problem the more confused we become.

Finally, we briefly discuss the cost of our simulations, all of which were done in memory on the CRAY-1. Without subcycling, the $Re = 200$ case, at $\Delta t = 0{\cdot}05$, cost 8·2 s CPU per shedding cycle; a typical run required 1–2 min total CPU. (For $Re = 50$ and 25, Δt was 0·025 and 0·015, respectively, based on a diffusion stability limit).

1.3. Simulation of a heavy gas release

This last example concerns the simulation of the dynamics associated with the gravitational spread and vapour dispersion of LNG (liquefied natural gas) spills over variable terrain in the atmosphere. Since the NG (natural gas) density at its boiling temperature is significantly greater than that of the ambient air (by approximately 60 per cent), the use of the Boussinesq equations for modelling such flows is probably inappropriate.[29] We have therefore employed the generalized anelastic formulation described by Chan *et al.*[30] In addition to solving equations similar to (1), we also solved the species conservation equation for NG mass fraction (ω). Herein we are interested in assessing the effects of the various Gauss rules on the numerical results and computational costs.

A graded mesh consisting of 6400 elements ($40 \times 20 \times 8$) was used in the simulations, with a total of 7749 nodal points and approximately 45,000 equations. The initial condition for the simulation was a steady isothermal wind field (~3 to 4 m/s) without NG vapour. Constant diffusivities, typical of the planetary boundary layer (0·4 m^2/s vertically and 2·0 m^2/s horizontally), were used throughout the simulation. The boil-off of LNG was simulated as a source area over 12 of the 30 elements comprising the spill pond; see Figure 13. Over this area, a vertical injection velocity of ~0·1 m/s, along with a temperature of −160°C (NG boiling temperature), and a constant rate of NG mass flux were specified. Away from the source area, we used $\mathbf{u} = \mathbf{0}$ and $\partial T/\partial n = \partial \omega/\partial n = 0$ at the ground. The remaining boundary conditions employed were: specified $\mathbf{u}$, T, ω at the inlet plane, natural boundary conditions at the outlet, and symmetry conditions at the top and two lateral surfaces.

The problem was run with three different Gauss rules: (a) 2-point quadrature for all

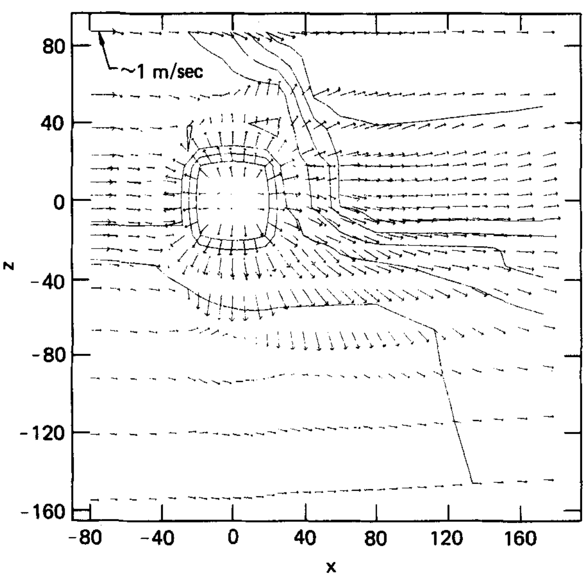

Figure 13. Horizontal velocities 1 m above the ground; 104 s after initiation of LNG spill. The spill pond is centred at (0, 0)

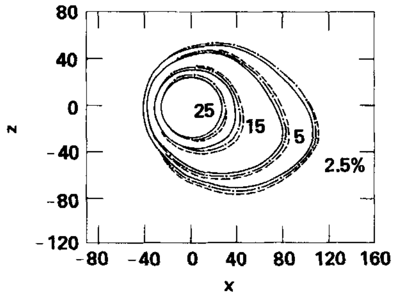

Figure 14. Predicted concentrations 1 m above the ground: —— 2-point; —·— mixed; - - - - 1-point

integrals, (b) mixed quadrature, namely 1-point quadrature for advection and diffusion, but 2-point quadrature for the others and (c) 1-point quadrature for all terms. The velocity field (plus terrain contours) 1 m above the ground at 104 s after initiation of the spill is shown in Figure 13; the vector field looks virtually identical for all 3 runs. Figure 14 shows the concentration contours on a 'horizontal' plane 1 m above the ground and Figure 15 displays the corresponding contours on a longitudinal plane through the pond centreline, both at the same time (104 s). As seen in these Figures, although the effects of different Gauss rules are noticeable, the important characteristics of the cloud (i.e. the gravitational spread in all directions and the shift of the cloud centreline away from the mean wind direction, due to gravity and topographic effects, both of which have been observed in field experiment) are similarly predicted by all three schemes. Furthermore, the agreement between the schemes regarding the predicted flammable zone (5 to 15 per cent NG vapour) is also very good.

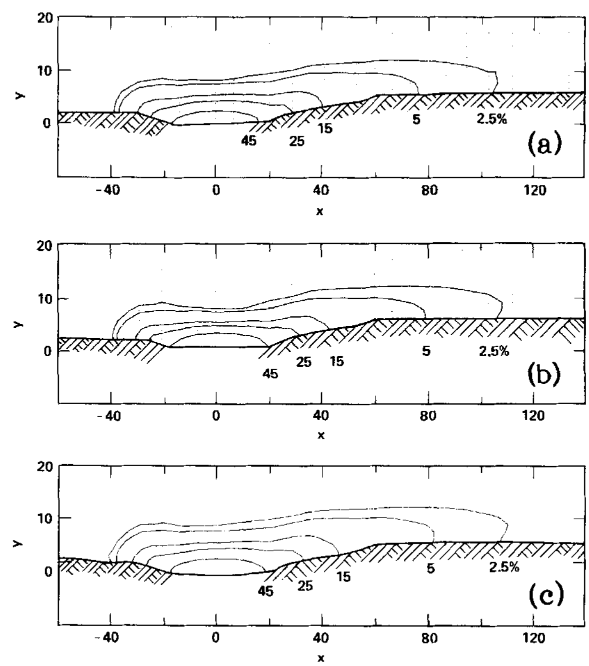

Figure 15. Predicted concentrations on a longitudinal plane: (a) 2-point, (b) mixed, (c) 1-point

Further and more detailed results of NG dispersion simulations are presented by Ermak *et al.*[31] and Chan *et al.*[30]

The code with 2-point quadrature (which must retrieve the advection and diffusion matrices from disc every time step and does not vectorize very well) required approximately 7 s of CPU and 13 s of I/O per time step to simulate 0·4 s of real time. The highly vectorized, 1-point quadrature code, on the other hand, required only 0·3 s of CPU and 1·3 s of I/O. The mixed quadrature approach required about 0·3 s of CPU and 1·8 s of I/O, with the additional I/O cost spent on retrieving the C matrix.

Further examples of results from this code are

(1) Transient lid-driven cavity, 2D and 3D.[32]
(2) Time-dependent 3D Benard convection with two different, oscillatory, 'steady-states'.[33]
(3) Time-dependent, stably-stratified lid-driven cavity, 2D and 3D.[34]
(4) Time-dependent 2D thermal convection of liquid metal (low Pr).[35]
(5) Comparison with laboratory data (3D) for isothermal and stratified lid-driven cavities.[36]

2. DISCUSSION

2.1. Steady-state, stability, subcycling and normal modes

An interesting side-effect of the velocity adjustment process associated with subcycling is worth some discussion. Each time the subcycled velocity is projected back onto the divergence-free subspace, the otherwise (nearly) continuous (in time) simulation is slightly perturbed. The consequences of this random-like perturbation are usually, but not always, innocuous. On occasion, however, the effects are quite noticeable and seem to be related to a sort of 'periodic' excitation of the system's 'normal modes'. This effect, which can probably also be regarded as a continuous application of a linear stability 'analysis' via small perturbations, is interesting but often annoying—especially when the flow is trying to approach a steady state. When these situations occur, and a steady-state is sought, we often turn off the subcycling option, after which the normal mode oscillations gradually decay.

For example, the lid-driven cavity solution at $Re = 10{,}000$ displayed some relatively large oscillations, at a dominant period of $\sim 1{\cdot}4$ (with a 'subharmonic' at a period of about 35), as 'steady-state' was approached—but the 'large' amplitudes occurred *only* in a small portion of the grid, namely in the region of the two lower right corner eddies (those, in fact, whose final shape, attained only after ~ 50 time units after subcycling was discontinued, disagreed somewhat with that presented by Ghia *et al.*[2]). It seems that these eddies are less stable, in some sense, and the perturbations caused them to shift back and forth, slightly changing size and shape with a period of $\sim 1{\cdot}4$. Also, there is no obvious correlation of these periods with the time steps employed: the minor Δt was 0·005 and the major Δt was $\sim 0{\cdot}13$ during these 'subcycle jitters', yet the amplitude and frequencies of the normal mode oscillations were quite constant. Finally we note that Koseff and Street[10] have observed that the transition from laminar flow to a semi-turbulent flow, which occurs in the Re range of 6000–8000 in a 3-D cavity, begins in this same region of the cavity. This might *not* be coincidental.

Another example, perhaps more easily explainable, can occur during a simulation involving a stably-stratified flow. In this case the normal modes include a wide spectrum of internal gravity waves; these are sometimes excited by the velocity adjustment process, but usually only to $O(\varepsilon)$ and usually only as a quasi-steady state is approached.

Thus, although subcycling is no panacea it is, on balance, very helpful; it cures more problems (excessive cost) than it causes, even though we must occasionally turn it off to see the 'truth'. It seems to have the potential, perhaps with further development, of becoming more useful and robust.

2.2. *2D vs 3D solution strategy*

Although we now routinely, and rather confidently, attack new 2D problems with the knowledge that we can generate a reasonably accurate and affordable simulation, 3D problems are still another matter. The basic difference between the two is that 2D problems can (usually) be solved completely in memory on the CRAY-1, whereas (essentially) all 3D problems require peripheral storage (on disk) of the factored pressure matrix. Although the CRAY-1 is impressively quick in CPU operations, it reads data from disk at a relatively very slow rate (~0·5 million words per second). Thus in a 3D simulation wherein the factored A matrix may require 1–10 million words (or more, for fine meshes), the CPU 'sits idle' for too many seconds while this matrix is read into memory—four times per major time step (once for a forward reduction and again for a back substitution, first for λ and then for P), in spite of the fact that CPU and I/O operations are overlapped as much as possible. Although subcycling is often especially effective in reducing costs in 3D, we believe that Gaussian elimination may need to be replaced if large problems are to be solved routinely. For example, Gresho and Upson[34] reported a cost of ~1 hour CPU and ~2·5 hours I/O to simulate 1 hour of real time (~14,000 minor steps and ~400 major steps) in a 3D lid-driven cavity flow using a coarse mesh ($18\times22\times16$ elements and ~2 million words for the A matrix) and that the I/O cost would have been a ridiculous 35 hours without subcycling. In contrast, the CPU cost associated with computing λ and P is a reasonably small fraction (~10–30 per cent) of the total CPU cost, i.e. the actual 'number crunching' associated with Gaussian elimination is not too expensive.

Thus, although we feel we can now afford to perform some 'simple' (<10,000 elements and short time) 3D calculations, it is clear that we are seriously hindered when it comes to long-time simultations of difficult problems (i.e. fine mesh), and that the main problem is caused by the tremendous I/O associated with Gaussian elimination.

Current research is accordingly directed toward solving the Poisson equation using methods less demanding of storage, i.e. iterative methods. Highest on our list of candidates is the conjugate gradient method, in one form or another (e.g. preconditioned; the multigrid method may also be viable). We hope to report success in this direction in the not-too-distant future.

3. CONCLUSIONS

(1) The techniques presented herein have provided a means for obtaining accurate and affordable, truly time-dependent solutions to the incompressible Navier–Stokes equations (and variants), at least in 2D. (3D solutions are either less accurate or less affordable—but still possible.)
(2) They are also useful for finding steady solutions, and will only do so when the solution exists. (Streamline upwinding is a natural and cost-effective adjunct for steady state simulations.)
(3) Balancing tensor diffusivity (BTD) is essential for cost-effective solutions to AD and/or NS when explicit Euler is used and the flow is advection-dominated.
(4) Subcycling is beneficial when the time step required for stability is much less than that required for accuracy.

(5) The hour-glass correction for short waves is often very useful and, sometimes, necessary.
(6) One-point quadrature is a cost-effective modification to GFEM when the simplest element is used. In 2D, element mass balances are assured and most problems can be solved in memory on modern computers such as the CRAY-1. (Mass lumping and explicit Euler also contribute to this cost-effectiveness.) In 3D, it may be advisable (in general) to use 2-point quadrature on the C-matrix.
(7) For transient simultations, the loss in accuracy owing to mass lumping is much greater than that caused by 1-point quadrature. For steady state simultations, mass lumping is not an issue (it is irrelevant).
(8) Some of the ideas presented herein (BTD, hourglass correction, subcycling) would presumably also be useful in some finite difference codes.
(9) Steady laminar flow in a 2D lid-driven cavity is stable for $Re \leq 10{,}000$ (the stability limit remains to be found).

ACKNOWLEDGEMENTS

Many people have contributed to the development of our current method: Dr. A. C. Hindmarsh (LLNL) has contributed extensively in the areas of stability and accuracy analysis, ODE theory, and linear algebra; Prof. R. L. Sani (University of Colorado) has been a continuous asset in nearly all relevant areas from physics through numerics; Dr. J. O. Hallquist (LLNL) helped us to understand and control the hour-glass modes; Dr. S. Sackett (LLNL) generated a special in-core (memory-contained) version of the FISSLE code for us and provided general consultation in its use; Dr. M. J. P. Cullen (British Met. Office) contributed to our understanding of $2\Delta x$ waves and pressure gradient errors; finally, Prof. A. J. Chorin (University of California, Berkeley) pointed out a better way to interpret and analyse the velocity adjustment process. We also thank Carol Myers for her skillful combination of typing and tolerance. This work was performed under the auspices of the U.S. Department of Energy by the Lawrence Livermore National Laboratory under contract No. W-7405-Eng-48.

REFERENCES

1. P. M. Gresho, S. T. Chan, R. L. Lee and C. D. Upson, 'A modified finite element method for solving the time-dependent incompressible Navier–Stokes equations. Part 1:Theory,' *Int. J. Num. Meth. Fluids*, **4**, 557–598 (1984).
2. U. Ghia, K. Ghia and C. Shin, 'High-*Re* solutions for incompressible flow using the Navier–Stokes equations and a multi-grid method', *J. Comp. Phys.*, **48**, 387 (1982).
3. R. Sani, P. Gresho, R. Lee and D. Griffiths, 'The cause and cure (?) of the spurious pressures generated by certain FEM solutions of the incompressible Navier–Stokes equations', *Int. J. Num. Meth. Fluids*, **1**, 17–43, 171–204 (1981).
4. O. Burggraf, 'Analytical and numerical studies of the structure of steady separated flows', *J. Fl. Mech.*, **24**, (1), 113 (1966).
5. J. Koseff, R. Street and H. Rhee, 'Velocity measurements in a lid-driven cavity flow', *Proceedings, ASME Conference on Numerical & Experimental Investigations of Confined Recirculating Flows*, 1983.
6. H. Moffatt, 'Viscous and resistive eddies near a sharp corner', *J. Fl. Mech.*, **18**, (1964).
7. K. Winters and K. Cliffe, 'A finite element study of driven laminar flow in a square cavity', *AERE Harwell Report R-9444*, 1979.
8. G. Batchelor, *An Introduction to Fluid Dynamics*, Cambridge University Press, Cambridge, 1967.
9. A. G. Hutton, 'Finite element boundary techniques for improved performance in computing Navier–Stokes and related heat transfer problems', in R. H. Gallagher *et al.* (eds) *Finite Elements in Fluids, vol. 4*, Wiley, Chichester, 1982, Chap. 20.
10. J. Koseff and R. Street, 'Visualization studies of a shear-driven three-dimensional recirculating flow', *Proc. ASME Symp. on Three-Dimensional Turbulent Shear Flows*, St. Louis, MO, 1982.

11. A. Brooks and T. Hughes, 'Streamline upwind/Petrov Galerkin formulation for convection-dominated flows with particular emphasis on the incompressible Navier–Stokes equations', *Comp. Meth. Appl. Mech. Eng.*, **32,** 199 (1982).
12. P. Gresho, R. Lee and R. Sani, 'On the time-dependent solution of the incompressible Navier–Stokes equations in two and three dimensions', in *Recent Advances in Numerical Methods in Fluids*, vol. 1, Pineridge Press, Swansea, U. K., 1980, p. 27.
13. P. Gresho, R. Lee and C. Upson, 'FEM solution of the Navier–Stokes equations for vortex shedding behind a cylinder: experiments with the four-node element', *Adv. Water Resources*, **4,** 175 (1981).
14. S. Jordan and J. Fromm, 'Oscillatory drag, lift, and torque on a circular cylinder in a uniform flow', *Phys. Fluids*, **15,** (3) 371 (1972).
15. J. Swanson and M. Spaulding, 'Three dimensional numerical model of vortex shedding from a circular cylinder,' *Nonsteady Fluid Dynamics*, ASME, N.Y., 1978.
16. D. Tritton, 'Experiments on the flow past a circular cylinder at low Reynolds numbers', *J. Fl. Mech.*, **6,** (4), 547 (1959).
17. D. Tritton, *Physical Fluid Dynamics*, Van Nostrand Reinhold Co., N.Y., 177.
18. E. Berger and R. Wille, 'Periodic flow phenomena', *Ann. Rev. Fluid Mech.*, **4,** 313 (1972).
19. M. Zdravkovich, 'Smoke observations of a Karman vortex street', *J. Fl. Mech.*, **37**, (3) 491 (1969).
20. J. Gerrard, 'The wakes of cylindrical bluff bodies at low Reynolds number', *Phil. Trans. Roy. Soc.*, **288**, (1354) 351 (1978).
21. A. Perry, M. Chong and T. Lim, 'The vortex-shedding process behind two-dimensional bluff bodies', *J. Fl. Mech.*, **116,** 77 (1982).
22. M. Coutanceau and R. Bouard, 'Experimental determination of the viscous flow in the wake of a circular cylinder in uniform translation. Part 1. Steady flow', *J. Fl. Mech.*, **79,** (2) 231 (1977).
23. S. Bloor, 'The transition to turbulence in the wake of a circular cylinder', *J. Fl. Mech.*, **19,** 290 (1964).
24. D. Tritton, 'A note on vortex streets behind circular cylinders at low Reynodds numbers', *J. Fl. Mech.*, **45,** (1) 203 (1971).
25. E. Berger, 'The determination of the hydrodynamic parameters of a Karman vortex sheet from hot wire measurements at low Reynolds number', *Z. Flug.*, **12,** 41 (1964).
26. C. Friehe, 'Vortex shedding from cylinders at low Reynolds number', *J. Fl. Mech.*, **100,** 237 (1980).
27. M. Gaster, 'Vortex shedding from slender cones at low Reynolds number', *J. Fl. Mech.*, **38,** (3) 565 (1969).
28. M. Gaster, 'Vortex shedding from circular cylinders at low Reynolds numbers', *J. Fl. Mech.*, **46,** (4) 749 (1971).
29. B. Daley and W. Pracht, 'Numerical study of density-current surges', *Phys. Fluids*, **11,** (1) 15 (1968).
30. S. Chan, H. Rodean and D. Ermak, 'Numerical simulations of atmospheric releases of heavy gases over variable terrain', in *Air Pollution Modeling and Its Application III*, 295, 1984.
31. D. Ermak, S. Chan, D. Morgan and L. Morris, 'A comparison of dense gas dispersion model simulations with Burro series LNG spill test results', *J. Haz. Mat.*, **6,** 129 (1982).
32. P. Gresho, C. Upson, S. Chan and R. Lee, 'Recent progress in the solution of the time-dependent, three-dimensional, incompressible Navier–Stokes equations', in T. Kawai (Ed.) *Finite Element Flow Analysis*, University of Tokyo Press, Tokyo, Japan; also UCRL-87362.
33. C. Upson, P. Gresho, R. Sani, S. Chan and R. Lee, 'A thermal convection simultation in three-dimensions by a modified finite element method', in *Numerical Properties and Methodologies in Heat Transfer, Proceedings of the Second Int. Symp.*, Hemisphere Publ. Corp., Washington, DC, 1983. Also UCRL-85555.
34. P. Gresho and C. Upson, 'Current progress in solving the time-dependent, incompressible Navier–Stokes equations in three dimensions by (almost) the FEM', *Proceedings, Fourth Int. Conf. on Finite Elements in Water Resources*, Hanover, Germany 21–15 June 1982. Also, UCRL-87445.
35. P. Gresho and C. Upson, 'Application of a modified finite element method to the time-dependent thermal convection of liquid metal', *Proceedings, Int. Conf. Num. Meth. Laminar and Turbulent Flow*, University of Washington, 8–11 August 1983.
36. J. Koseff, R. Street, P. Gresho, C. Upson, J. Humphrey and W. To, 'A three-dimensional lid-driven cavity flow: experiment and simulation, *Proceedings, Int. Conf. Num. Meth. Laminar and Turbulent Flow*, University of Washington, 8–11 August 1983.